

**Internal Structure and Expansion Dynamics
of Laser Ablation Plumes into Ambient Gases**

**S. S. Harilal, C. V. Bindhu, M. S. Tillack,
F. Najmabadi and A. C. Gaeris**

September 28, 2002



**Fusion Division
Center for Energy Research**

University of California, San Diego
La Jolla, CA 92093-0417

Internal Structure and Expansion Dynamics of Laser Ablation Plumes into Ambient Gases

S. S. Harilal, C. V. Bindhu, M. S. Tillack, F. Najmabadi, A. C. Gaeris
Center for Energy Research, University of California San Diego
9500 Gilman Drive, La Jolla, CA 92093-0417

The effect of ambient gas on the expansion dynamics of the plasma generated by laser ablation of an aluminum target has been investigated using frequency doubled radiation from a Q-switched Nd:YAG laser. The diagnostic tools include fast photography of overall visible plume emission using a 2 ns gated intensified CCD camera and space and time resolved emission spectroscopy using a 50-cm monochromator/spectrograph and PMT. The expansion behavior of the plasma was studied with ambient air pressure ranging from 10^{-6} Torr to 100 Torr. Free expansion, plume splitting and sharpening, hydrodynamic instability and stagnation of the plume were observed at different pressure levels. Space and time resolved emission spectroscopic studies showed a twin peak distribution for Al and Al⁺ species at farther distances illustrating plume splitting at pressures higher than 100mTorr. Combining imaging together with time resolved emission diagnostics, a triple structure of the plume was observed. The expansion of the plume front was compared with various expansion models and found to be generally in good agreement.

Key Words: Laser produced Plasma, Fast Photography, Plume Splitting, Optical emission spectroscopy, Background gas effects

PACS: 52.38, 52.50.Jm, 52.70.Kz

1. Introduction

Laser-produced plasma is transient in nature with characteristic parameters that evolve quickly and are strongly dependent on irradiation conditions such as incident laser intensity and pulse duration, laser wavelength, irradiation spot size, ambient gas composition and ambient pressure¹⁻⁷. The different mechanisms involved during a laser ablation process, including laser absorption, evaporation, transient gas dynamics, radiation transport, condensation, ionization and recombination, are rather complex and require further investigation.

There are several diagnostic techniques for characterizing a laser produced plasma including optical emission spectroscopy⁸⁻¹⁰, mass spectroscopy¹¹, laser induced fluorescence¹², Langmuir probe¹³, photo-thermal beam deflection¹⁴, microwave and laser interferometry^{15,16}, and Thomson scattering¹⁷. Fast photography adds another dimension to ablation diagnostics by providing two-dimensional (2D) snap shots of the three-dimensional (3D) plume propagation¹⁸⁻²⁰. This capability becomes essential for a hydrodynamic understanding of the plume propagation and reactive scattering.

The interaction of pulsed laser ablation plumes with a background gas has received increased attention recently due to its importance in laser deposition²¹, nanoparticle formation and growth²², cluster production²³ etc. In addition to these applications, these studies are very important for modeling of various processes in space physics, plasma chemistry and hydrodynamics. Compared to the expansion into a vacuum, the interaction of the plume with an ambient gas is a far more complex gas dynamic process due to the rise of new physical processes involved such as deceleration, attenuation, thermalization of the ablated species, diffusion, recombination, formation of shock waves and clustering^{2,6,10,24-27}. Recent measurements performed over a wide range of expansion durations have described a fairly complicated gas dynamic picture of plume ambient gas interaction which is characterized by different propagation phases and is accompanied by plume oscillations arising at rather high background pressures^{10,28,29}. In low gas pressure (less than 100 mTorr), the plume expansion could be described by Monte Carlo simulation^{30,31}. For high pressures many numerical simulations were performed using compressible and nondissipative conservation equations (Euler)³². However, for Euler modeling, all the simulated species including the neutral atoms and ions have the same velocity, whereas experimental results indicate that excited neutral particles are characterized by slower velocity in comparison with ionized atoms²⁹. In moderate or high pressures, a blast wave model is found to describe accurately the plume propagation distance during the early expansion stages, whereas a

shock layer model and an empirical drag model predict the maximum plume length with considerable accuracy²⁶.

The emission spectra, electron temperature and density are found to be significantly influenced by the ambient atmosphere⁶. As discussed by several authors, the surrounding atmosphere also affects the crater size³³ and the amount of sample vaporized with the laser beam³⁴. The relative enhancement of an emitted line depends on the nature of the gas, gas pressure and the excitation energy of the electronic transition responsible for the line⁶. The two main mechanisms invoked in the excitation are the particle collision excitation and the electron impact excitation. Although extensive experimental and theoretical work have been done, many effects of the laser beam interaction with a metallic surface in the presence of ambient gas are still not satisfactorily explained³⁵⁻⁴⁰.

In this paper, we present a detailed experimental analysis of the laser ablation of aluminum by 2-ns gated photography and space and time resolved emission spectroscopy. Fast side-on views of the plume expansion are made by recording overall visible emission from the plasma plume, which enable us to obtain information on the interaction of the plasma with the ambient gas during earlier and later stages of the process. Investigations are made on the stratification and stability of the geometry and shape of the aluminum plasma at different air pressures ranging from 10^{-6} Torr to 100 Torr. We report plume splitting in the fast moving component of the plasma plume, which, to the best of our knowledge, has never been reported. The plume splitting behavior appears only in a narrow region of pressure (around 150mTorr). Spatially resolved Time of Flight (TOF) emission measurements are carried out at this pressure to infer the species local populations inside the plasma. Present results indicate that the combination of fast photography and time resolved emission spectroscopic diagnostic techniques gives much more insight into the expansion behavior of a laser produced plasma into an ambient atmosphere. We also estimated the ion stopping distance using the popular Monte Carlo Simulation model^{41,42} (SRIM code) and compared with our experimental data. An adiabatic expansion model is used to describe the plume length of the laser created aluminum plasma at different ambient pressures.

2. Experiment Description

The schematic of the experimental set up is given in figure 1. Pulses from a frequency doubled Nd:YAG laser (8 ns pulse width, maximum energy 700 mJ) were used to create aluminum plasma in a stainless steel vacuum chamber. The chamber was pumped using a high-speed turbo-

molecular pump and a maximum base pressure $\sim 10^{-8}$ Torr was achieved. The aluminum target in the form of a disk was rotated about an axis parallel to the laser beam. This avoids errors due to local heating and drilling. The laser beam was attenuated by a combination of wave plate and cube beam splitter and focused onto the target surface at normal incidence using an antireflection-coated plano-convex lens. The beam energy was monitored using an energy meter (Ophir, Model 30A).

The plume imaging was accomplished using an intensified CCD camera (PI MAX, Model 512 RB) placed orthogonal to the plasma expansion direction. A Nikon lens was used to image the plume region onto the camera to form a 2-dimensional image of the plume intensity. The visible radiation from the plasma was recorded integrally in the wavelength range 350-900 nm. In order to eliminate 532 nm stray photons reaching the camera, a magenta subtractive filter was used. A programmable timing generator was used to control the delay time between the laser pulse and the imaging system with overall temporal resolution of 1 ns.

For space and time resolved spectroscopy, an optical system was used to image the plasma plume onto the entrance slit of the monochromator/Spectrograph (Acton Pro, Spectra-Pro 500i), so as to have one-to-one correspondence with the sampled area of the plume and the image. The optical system was translated to monitor different parts of the plume. Spatial resolution provided by our optical system was better than 0.5 mm. The monochromator was equipped with 3 gratings: 150 g/mm, 600 g/mm and 2400 g/mm. One of the exit ports of the spectrograph was coupled to an intensified CCD camera that was operated with vertical binning of the CCD array to obtain spectral intensities *vs* wavelength. The other exit port of the monochromator was coupled to a photomultiplier tube (PMT). A diverter mirror was used for switching from PMT to ICCD or vice versa. For time resolved studies of a particular species in the plume, the specific lines are selected by tuning the grating and imaging onto the slit of the PMT. For recording the temporal profiles, the output of the PMT was directly coupled to a 1GHz Digital Phosphor Oscilloscope (Tektronix TDS5014, 5 GS/s maximum real-time sample rate). This set up provides delay as well as decay of emission of a constituent species within plasma which are very important parameters related to the evolution of laser-ablated materials in a direction normal to the target surface.

3. Physical description of Laser Plasma Expansion

Since the laser intensity exceeds the ablation threshold of the target, the laser beam evaporates and ionizes material, creating a plasma plume above the material surface. Initially the atoms, molecules and ions undergo collisions in the high-density region near the target forming the so-called

Knudsen layer, leading to a highly directional expansion perpendicular to the target. The expansion dynamics of the laser-produced plasma plume have been described elsewhere using semiquantitative models^{43,44}. In the initial stage, the interaction of the laser beam with the bulk target results in the evaporation of the surface layer. Following this, the interaction of the laser beam with the evaporating material leads to the formation of an isothermally expanding plasma and this persists until the termination of the laser pulse. The vapor particles are pushed forward and in the lateral direction solely by high pressure emanating from the target surface when the ejected plume is considered transparent to the incident laser beam. Strong laser-plasma interaction creates an additional high-pressure kinetic energy region fuelling further expansion of the plume. After the termination of the laser pulse, no particles are ejected from the target surface. An adiabatic expansion of the plasma occurs where the temperatures can be related to the dimensions of the plasma. Singh and Narayan⁴³ have found that the forward directed nature of the laser evaporation process results from anisotropic expansion velocities of different species, which are mainly controlled by the initial dimensions of the expanding plasma. The thermal energy is rapidly converted into kinetic energy, with the plasma attaining extremely high expansion velocities. During the initial stages of plasma expansion when the particle density is high ($\sim 10^{19} \text{ cm}^{-3}$), the mean free path of the particles is short ($\sim \mu\text{m}$) and the plasma behaves as a continuum fluid. As the plasma expands the temperature drops very rapidly (within 100 ns time), however the drop is smaller at later times ($>100 \text{ ns}$) because energy is regained in the recombination of ions.

The plasma expands freely in vacuum or low background pressures. As the background pressure increases, the plume behavior is characterized by strong interpenetration of the laser plasma and ambient low-density gas. The expansion dynamics of the plume in this pressure regime is determined by the properties of the plasma as well as the background gas. In this regime collisional effects starts to play a role. At still higher background pressures, the expansion dynamics of the plasma are fully governed by the nature and pressure of the ambient gas used²⁶. In general, an increase in background pressure results in the following effects: (i) an increase in fluorescence from all species due to enhanced collisions on the expansion front and subsequent inter-plume collisions, (ii) shock front formation, (iii) slowing of the plume compared to propagation in vacuum resulting in spatial confinement of the plasma. The presence of ambient gas during expansion may also lead to reactive scattering, thermalization of the plume, enhanced condensation leading to cluster and nanoparticle formation, *etc.*

4. Imaging results and Analyses:

Plasma emission begins on the target surface soon after the laser photons reach the surface. Images of the time evolution of the expanding aluminum plasma were taken at different air pressures ranging from 10^{-6} Torr to 100 Torr. Typical ICCD images of the expanding plume at different times after the onset of plasma are given in Figures 2-7 at different air pressures. These images were recorded at a laser irradiance of 3 GW cm^{-2} . The duration of the intensification (exposure time) is 2 ns and each image is obtained from a single laser pulse. Timing jitter is less than 1 ns. All of the images given in the figures are normalized to the maximum intensity in that image. It should be remembered that each image represents the spectrally integrated plume in the region 350-900 nm that is due to emission from the excited states of various species. They are not necessary representative of the total flux because a part of the plume is nonluminous.

Figs. 2 and 3 represent the plume expansion at 10^{-6} Torr and 2×10^{-2} Torr respectively. From the figures, it is clear that there is not much influence of the ambient air pressure on the expansion of the plasma when we increase air pressures from 10^{-6} to 2×10^{-2} Torr. In this region, the plasma expands freely. Plasma expansion into a vacuum environment is simply adiabatic and can be fully predicted by theoretical models and numerical gas dynamic simulations⁴³. If the particles are released and the number of collisions among them are not too high, the Knudsen layer feeds an unstable adiabatic equilibrium (UAE)^{45,46}. The UAE may evolve in a steady adiabatic flow, which terminates due to falling density with time. The light emission from the plume very close to the target surface exists even after 1 μs . This stationary emission region close to the target surface has been reported by others¹⁸ and may result from gas collisions between the plume ejecta in the high pressure region of the initial expansion, resulting in a Knudsen layer with stopped and/or backward moving material⁴⁶.

When the pressure is increased to 10^{-1} Torr, the plume breaks away from the target surface 70 ns after the onset of the plasma, forming a faster moving component and a slow moving/stationary component near the target surface. Coincidentally, this pressure range falls within the transition from collisionless to collisional interaction of the plume species with the gas. This is supported by the fact that at these pressure levels the intensity of radiation is enhanced especially after 100ns. Here the plume behavior is characterized by strong interpenetration of the laser plasma and ambient low-density gas, where a contact boundary is formed between plasma and a shock wave in the gas. During interpenetration, the transfer of kinetic energy from laser plasma to the background gas takes place and energy and momentum exchange occurs because of

ion-ion Coulomb scattering, ion-neutral collisions, charge exchange interactions etc. The emission of this component exists until 1500 ns from the beginning of the expansion process. The time evolution of the plume at a background pressure of 150 mTorr is given in figure 4. At early times, the plume front is spherical in nature, but as time evolves, the plume front becomes sharpened. Plume sharpening behavior suggests that higher kinetic energy particles are emitted closer to the target surface normal. It has been reported that ions of highest ionization state dominate in the direction of maximum emission, and that their concentration falls sharply away from the normal⁴⁷. Along with sharpening, the faster moving component of the expanding plume front splits again into two clouds indicating plume splitting. These peculiar plume splitting and sharpening phenomena are observed only in a particular pressure range (around 150 mTorr). Several authors have reported plume splitting in a laser produced plasma using ion probe³⁰, time of flight (TOF) mass spectroscopy¹¹, optical emission spectroscopy²⁸, laser induced fluorescence⁴⁸ etc. On the contrary, we observed plume splitting in the faster moving component in imaging studies, which as far as we know, is the first such observation. Here the fast component of the plume has penetrated into ambient gas and a part of it may be decelerated because of interaction with background gas.

As we increase the pressure from 10^{-1} Torr, the mutual penetration of the laser plasma ions and the ambient gas decreases and an interface is formed. In this regime, along with deceleration, turbulence also appears in the expanding plume. The time evolution of the images of the plume at 1.3 Torr air pressure are given in figure 5. Here also the fast component of the plume penetrates into the ambient gas and the instability is observed mostly in the slower component. We expect that near the contact boundary instabilities such as Rayleigh –Taylor (RT) set in the plasma. Baranov et. al³⁵ addressed instability of a laser produced expanding plasma in a background gas. According to them, due to RT instability, the expanding plume front tends to become unstable and the interface between the plasma and ambient gas becomes perturbed. The turbulence stage was enhanced at a pressure range around 1 Torr where we can see a number of intensity peaks. This turbulence appeared after 200 ns after the evolution of the plume (for a background pressure of 1.3 Torr) and the instability was manifested by breaking up of radiation. We also confirmed that the occurrence of heated spots in the plume is not merely due to reactive processes inside the plume (*e.g.*, formation of AlN or AlO) by introducing He and Ar as background gases. We still observe the instability during plume expansion into Ar and He background gases, but at different pressure levels.

We made an estimate of the density of the background gas where the RT instability can form in the present experimental conditions. The RT instability would grow exponentially with time, $\sim e^{\eta t}$, at a rate⁴⁹

$$\eta^2 = ka \frac{(\rho_p - \rho_b)}{(\rho_p + \rho_b)} \quad (1)$$

Where ρ_p and ρ_b are the density of the plasma and background gas respectively, $a = dv/dt$, v being the velocity of the plasma front and k is a perturbation wave number. The plasma boundary is stable when $\eta^2 > 0$ ($\rho_p > \rho_b$) while the arrangement becomes unstable when $\eta^2 < 0$ ($\rho_p < \rho_b$). The instability growth occurs in the maximum acceleration region that can be derived from the derivative of momentum conservation equation

$$\frac{d}{dt} \left[\left(M_0 + \frac{4}{3} \pi R^3 \rho_b \right) v \right] = 0 \quad (2)$$

where M_0 is the laser plasma mass, R is the distance from the target surface. The growth of instability corresponds to maximum acceleration region and from equation (2),

$$R = \left(\frac{3M_0}{4\pi\rho_b} \right)^{1/3} \quad (3)$$

Following Ng. et al⁵⁰, the mass ablated in the present experimental conditions is estimated to be 1.71×10^{-5} g. Using our experimental parameters, viz. $R = 1.3$ cm, the calculated background density is 1.87×10^{-6} g cm⁻³ which corresponds to a pressure of 1.22 Torr (considering nitrogen) which is in good agreement with the experimental observation.

As the pressure increases, plasma deceleration starts more rapidly because of confinement of plume. The plume expansion behavior at 10 Torr and 100 Torr are given in figures 6 and 7 respectively. At these pressure levels, the plasma deceleration starts very early. The expansion front is slowed more rapidly and coalesces with the slower components. As the pressure of the ambient gas increases, greater confinement of the plasma takes place and the effective length of the plume is reduced to a few millimeters. The lifetime of the plasma plume is found to be much higher in this pressure regime because of the formation of different molecules like AlO, AlN etc.⁵¹ that have much higher decay time compared to neutral and ionic species.

In order to have a better understanding of the plasma expansion and evolution, we used the imaging data to create position-time plots of the luminous front at several background air pressures shown in figure 8. The symbols in the figure represent experimental data points and the curves represent different expansion models. At low pressures ($< 10^{-2}$ Torr) the plume front behaves

linearly with time (the straight-line fit in the graph corresponds to $R \propto t$). This indicates free expansion of the plume into vacuum. The expansion velocities of the plasmas are measured from the slopes of the displacement–time graph. The estimated expansion velocities of the plasma in this pressure region is $\sim 10^7 \text{ cm s}^{-1}$ which is the same as the free expansion velocity. Plume expansion in the early stage ($< 40 \text{ ns}$) is almost linear irrespective of the background gas pressure. The plume expansion at moderate pressures is represented by a shock model given by^{26,52}

$$R = \xi_0 (E_0/\rho_0)^{1/5} t^{2/5} \quad (4)$$

where ξ_0 is a constant which depends on γ , the specific heat capacity. The shock model describes the explosive release of energy E_0 through a background gas of density ρ_0 . The shock model, which neglects viscosity, gives a prediction of complete propagation. As shown in fig. 8, the plume front position with time for 1.3 Torr agrees well with the shock model.

At later stages the plume expansion is described by a drag model, which is given by

$$R = R_0(1-\exp(-\beta t)) \quad (5)$$

where R_0 is the stopping distance of the plume and β is the slowing coefficient ($R_0\beta = v_0$). The drag model predicts that the plume will eventually come to rest due to resistance from collisions with the background gas. The plume front position at later stages ($> 500 \text{ ns}$) is well described by the drag model (fig.8). The plume front position of the plasma at 150 mTorr showed a $t^{0.445}$ dependence.

Plume Length

We tried to estimate the length of the plume at different ambient gas pressures using an adiabatic expansion model and the range of Al ions using a Monte Carlo Simulation program. According to the adiabatic expansion model⁴, the ablated species pushes the background gas species until the plasma and gas pressure equilibrate. Then the length of the plasma is given by

$$L = A[(\gamma-1)E]^{1/3\gamma} P^{-1/3\gamma} V^{\gamma-1/3\gamma} \quad (6)$$

where A is the geometrical factor related to the shape of the laser spot at the target surface, γ is the specific heat ratio, E is the laser energy, P_0 is the ambient gas pressure, V is the initial volume of the plasma is given by $V = v_0 \tau_{\text{laser}} w$ (where v_0 is the initial species velocity, τ_{laser} is laser pulse width and w is the spot size at the target surface). The factor A depends on the expansion geometry and for a conical plume with an expansion angle θ (circular spot)

$$A = \left(1 + \frac{1}{\tan \theta}\right) \left(\frac{3 \tan \theta}{\pi + 2\pi \tan \theta}\right)^{1/3} \quad (7)$$

Considering experimental parameters with $\theta = 30^\circ$, the estimated values of plume length at different pressures along with experimental maximum range of the plume are given in fig. 9 which is fairly in good agreement with the experimentally observed plume lengths (taken from ICCD images). Both the experiment and the model reveal that the ambient gas slows down the expansion of the ablation plume.

The estimate of mean projected length of Al^+ ions at different ambient pressures of air is based on the popular Monte Carlo simulation program SRIM^{41,42}. The calculated results are also given in fig. 9. The estimated stopping distance is in good agreement with experimentally observed value of plume length at low pressure (around 150mtorr). The calculations did not follow experimental values at high pressures, where the plume length is found to be much higher compared to the calculated Al^+ ion range. The comparison shows that the Monte Carlo simulation model is good for low pressures only.

5. Spectroscopic Results and Plume Splitting

To gain more insight, we performed space and time resolved spectral emission studies of different species in the expanding plasma in the background pressure levels described above. Measurements of the temporal locations of the maximum intensity as a function of distance give an estimate of the velocity component perpendicular to the target surface.

Our spectroscopic studies show that most of the species emitted by laser produced aluminum plasma in the present experimental conditions are excited neutral Al species along with Al^+ and Al^{++} . Time resolved studies were made for Al (396.1 nm , $3s^2 ({}^1\text{S})3p - 3s^2 ({}^1\text{S})4s$) and Al^+ (358.6 nm , $3s3d - 3s4f$) species in the plasma at different distances from the target surface.

The expansion velocities of the kinetic peaks are strongly affected by the background gas pressure. Gas phase collisions can transform the initial temporal distributions into a very different final distribution. With increasing pressure, due to the enhanced collision with the background gas species, the slowdown process is very rapid. Thus the ambient gas acts as a retarding media, slowing the plume development and the bringing the ion energy closer to the energy of excited neutral atomic species in the plasma. At low pressures, the temporal profiles of the different emitting species are described by single peak distribution. But, as the pressure increases, we find that the temporal distribution of excited Al and Al^+ is changed to a twin peak distribution. In this section, we particularly emphasize the double peak observation in the temporal profiles of Al and

Al⁺ species at 150 mTorr pressure, where the plume splitting appeared during later stages of the plasma expansion.

The time evolution of the spectral emission profiles obtained in the present work clearly reveals that the species ejected by the Al plume exhibit twin peaks for the TOF distribution. Figure 10 shows the typical TOF profile of Al at 396.1 nm recorded at a distance 18 mm from the target surface at a background pressure of 150 mTorr. The twin-peak distribution is observed only beyond a certain distance from the target. The R-t plots are drawn for Al and Al⁺ species are given in figs. 10 and 11 respectively. It is interesting to note that the faster peak for excited Al and Al⁺ species propagate without much attenuation. The estimated expansion velocities of fast moving Al⁺ and Al species are $7.6 \times 10^6 \text{ cms}^{-1}$ and $6.5 \times 10^6 \text{ cms}^{-1}$ respectively which correspond to a kinetic energy of 800 eV and 650 eV. It is expected that fast electrons and ions travel at the leading edge of the plume. The ions can scatter the ambient gas, so that the following neutral particles propagate through a more rarefied ambient medium. The faster peak moves with a velocity very close to the free expansion velocity and the slower one follows a $t^{0.445}$ dependence that exactly matches with the plume front position corresponding to 150 mTorr as given in fig. 8.

Our measurements also show that (figs. 11 and 12) the higher the ionization state, the greater the kinetic temperature. This is probably due to enhanced absorption of laser light by the plasma. After the laser action ceases the charge composition of the plasma is governed by 3-body recombination, which dominates over radiative and/or dielectronic ones due to the rapid drop in electron temperature as the plasma expands. The ions located at the front of the plasma acquire the largest energy during hydrodynamic acceleration and the interaction time for recombination is very much reduced. This small group of high-energy ions transports a significant fraction of absorbed energy. The ions located in the inner plume layers are accelerated much less due to hydrodynamic expansion. They remain much longer in the denser state, which is being subjected to strong recombination, which in turn enhances the emission from these regions.

The position of the plume front recorded using ICCD imaging at 150 mTorr moves much slower than the free expansion model. The slow moving component in the TOF species matches well with the plume front position recorded using ICCD imaging. However, we see almost no signal corresponding to the faster profile in the TOF species using ICCD imaging studies. The TOF profiles indicate that the yield or concentration of the higher kinetic energy peak is rather low compared to the slow moving component, which leads us to believe that the dynamic range of the ICCD is not high enough to expose these photons.

Since we observe plume splitting with imaging studies for the low kinetic energy component in the TOF profile, we conclude that there exists a triple plume structure with one component traveling near vacuum speed and two other slower components. The estimated temporal separation at a specific spatial point (considering the image at 610 ns) in plasma between the two slow layers observed with the imaging studies is ~ 60 ns. The TOF distribution of the slow component is rather broadened, and hence we do not clearly see the splitting of the delayed TOF distribution as observed with the imaging studies. Only through the combination of imaging and TOF spectroscopy do we determine the full plume structure.

In order to gain more insight into the kinetic properties of the plume species, a shifted Maxwell-Boltzmann (SMB) distribution is used to fit the TOF profile of Al species. The SMB fit function is given by⁵³

$$f(v) = Av^3 \exp\left(-\frac{m(v-v_0)^2}{2kT}\right) \quad (6)$$

where A is the normalization parameter, v is the velocity of the species, v_0 is the flow velocity, T is the translational temperature and m is the mass of the species. Fig. 12 gives the best curve fit for the faster and slower kinetic peaks. There is a mismatch observed with the fitted SMB distribution for the slower peak. We expect that the second peak is a convolution of TOF profiles of the same species having different velocities. So we attempted to fit 2 SMB distributions in the slower peak and the superposition of these two fits gives relatively good agreement with the experimentally observed TOF curve.

6. Conclusions

The expansion dynamics of laser produced Al plasma has been studied using fast photography and space and time resolved emission diagnostic techniques. The time evolution of 2 ns gated photography employing an intensified CCD camera allowed a precise description of the aluminum plume evolution. The expansion behavior of the plasma at different ambient air pressures ranging from 10^{-6} torr to 100 Torr was studied. The results show several interesting effects.

At low ambient pressure levels ($<10^{-2}$ Torr), the plasma expands freely. The addition of ambient gas leads to more efficient electron impact excitation and plasma recombination which enhances the emission from different species in the plasma. As pressure increases above 100 mTorr, the plume is characterized by strong interpenetration of the plasma species and background gas that leads to plume splitting and sharpening. During this stage of mutual penetration of laser

plasma and ambient gas, a considerable fraction of kinetic energy was converted into heat which in turn increases the temperature of the gas and radiation. At pressure levels around 1 Torr, turbulence is observed in the decelerating plume front. A further increase in pressure resulted in contraction of the mutual penetration zone and the plasma front becomes compressed.

It is also noted that in the earlier stage (<40 ns) plasma expansion is almost linear irrespective of the background pressure. At moderate pressures and at times <500 ns, the plasma expansion is characterized by a spherical shock wave model. For time >500 ns, the velocity of the plume is low due to numerous collisions with the background gas molecules. The drag model is a good approximation in this regime. The results obtained with time of flight emission studies showed a twin peak distribution for Al and Al⁺ species indicating plume splitting. Here the faster component of the species moves with the free expansion velocity whereas the slowed component has characteristics which are strongly influenced by the pressure of the background gas.

Combining both the diagnostic tools, a triple structure of the plume is deduced. Highly energetic ions moving with the free expansion velocity are not observed with fast imaging studies, probably overlooked because of bright plume luminescence of the slow component. The temporal evolution of the slower component follows the plume front position recorded by fast photography.

An estimate of the plume and ion range is made for different ambient gas pressures using adiabatic expansion and Monte Carlo Simulation models. The plume length estimate using the adiabatic expansion model is in good agreement with observed plume length. The calculated ion range using the Monte Carlo simulation model shows good agreement with plume length measurements at moderate pressures, but considerable deviation is found at high pressures.

References:

- ¹ V. Bulatov, L. Xu, and I. Schechter, *Analytical Chemistry* **68**, 2966-2973 (1996).
- ² A. V. Bulgakov and N. M. Bulgakova, *Journal of Physics D* **28**, 1710-1718 (1995).
- ³ J. J. Chang and B. E. Warner, *Applied Physics Letters* **69**, 473-5 (1996).
- ⁴ P. E. Dyer, A. Issa, and P. H. Key, *Applied Physics Letters* **57**, 186-8 (1990).
- ⁵ J. Gonzalo, C. N. Afonso, and I. Madariaga, *Journal of Applied Physics* **81**, 951-5 (1997).
- ⁶ S. S. Harilal, C. V. Bindhu, V. P. N. Nampoory, and C. P. G. Vallabhan, *Applied Physics Letters* **72**, 167-9 (1998).
- ⁷ A. A. Voevodin, J. G. Jones, J. S. Zabinski, and L. Hultman, *Journal of Applied Physics* **92**, 724-735 (2002).

- 8 A. A. Voevodin, J. G. Jones, and J. S. Zabinski, *Journal of Applied Physics* **88**, 1088-1096 (2000).
- 9 S. Amoroso, R. Bruzzese, N. Spinelli, and R. Velotta, *Journal of Physics B* **32**, R131-72 (1999).
- 10 S. S. Harilal, *Applied Surface Science* **172**, 103-9 (2001).
- 11 S. M. Park and J. Y. Moon, *Journal of Chemical Physics* **109**, 8124-8129 (1998).
- 12 S. J. P. Laube and A. A. Voevodin, *Surface & Coatings Technology* **105**, 125-129 (1998).
- 13 R. M. Mayo, J. W. Newman, A. Sharma, Y. Yamagata, and J. Narayan, *Journal of Applied Physics* **86**, 2865-2871 (1999).
- 14 S. H. Jeong, R. Greif, and R. E. Russo, *Journal of Physics D* **32**, 2578-85 (1999).
- 15 D. Kim, H. K. Park, and C. P. Grigoropoulos, *International Journal of Heat and Mass Transfer* **44**, 3843-53 (2001).
- 16 T. Masubuchi, T. Tada, E. Nomura, K. Hatanaka, H. Fukumura, and H. Masuhara, *Journal of Physical Chemistry A* **106**, 2180-6 (2002).
- 17 S. H. Glenzer, K. B. Fournier, C. Decker, B. A. Hammel, R. W. Lee, L. Lours, B. J. MacGowan, and A. L. Osterheld, *Physical Review E* **62**, 2728-38 (2000).
- 18 D. B. Geohegan, *Applied Physics Letters* **60**, 2732-4 (1992).
- 19 S. S. Harilal, C. V. Bindhu, and H. J. Kunze, *Journal of Applied Physics* **89**, 4737-40 (2001).
- 20 S. S. Harilal, C. V. Bindhu, V. P. Shevelko, and H. J. Kunze, *Journal of Physics B* **34**, 3717-3726 (2001).
- 21 *Pulsed Laser Deposition of Thin films* (John Wiley & Sons, Inc., New York, 1994).
- 22 D. B. Geohegan, A. A. Puretzky, G. Duscher, and S. J. Pennycook, *Applied Physics Letters* **73**, 438-440 (1998).
- 23 H. W. Kroto, J. R. Heath, S. C. O'Brien, R. F. Curl, and R. E. Smalley, *Nature* **318**, 162-3 (1985).
- 24 O. B. Anan'in, Y. A. Bykovskii, E. L. Stupitskii, and A. M. Khudaverdyan, *Soviet Journal of Quantum Electronics* **17**, 1474-75 (1987).
- 25 A. V. Bulgakov and N. M. Bulgakova, *Journal of Physics D* **31**, 693-703 (1998).
- 26 D. B. Geohegan, in *Pulsed Laser Deposition of Thin Films*, edited by D. B. Chrisey and G. K. Hubler (John Wiley & Sons, Inc., New York, 1994), p. 115-165.
- 27 D. B. Geohegan and A. A. Puretzky, *Applied Physics Letters* **67**, 197-199 (1995).

- 28 S. S. Harilal, R. C. Issac, C. V. Bindhu, V. P. N. Nampoori, and C. P. G. Vallabhan,
Journal of Applied Physics **80**, 3561-3565 (1996).
- 29 S. S. Harilal, R. C. Issac, C. V. Bindhu, V. P. N. Nampoori, and C. P. G. Vallabhan,
Journal of Applied Physics **81**, 3637-3643 (1997).
- 30 R. F. Wood, J. N. Leboeuf, K. R. Chen, D. B. Geohegan, and A. A. Puretzky, Applied
Surface Science **129**, 151-158 (1998).
- 31 T. E. Itina, Nuclear Instruments & Methods in Physics Research Section B **180**, 112-116
(2001).
- 32 J. N. Leboeuf, K. R. Chen, J. M. Donato, D. B. Geohegan, C. L. Liu, A. A. Puretzky, and
R. F. Wood, Physics of Plasmas **3**, 2203-2209 (1996).
- 33 P. R. D. Mason and A. J. G. Mank, Journal of Analytical Atomic Spectrometry **16**, 1381-
1388 (2001).
- 34 R. E. Russo, X. L. L. Mao, M. Caetano, and M. A. Shannon, Applied Surface Science **96-8**,
144-148 (1996).
- 35 V. Y. Baranov, O. N. Derkach, V. G. Grishina, M. F. Kanevskii, and A. Y. Sebrant,
Physical Review E **48**, 1324-36 (1993).
- 36 R. C. Issac, G. K. Varier, P. Gopinath, S. S. Harilal, V. P. N. Nampoori, and C. P. G.
Vallabhan, Applied Physics A **67**, 557-561 (1998).
- 37 W. Pietsch, Journal of Applied Physics **79**, 1250-1257 (1996).
- 38 J. R. Ho, C. P. Grigoropoulos, and J. A. C. Humphrey, Journal of Applied Physics **79**,
7205-15 (1996).
- 39 M. Aden, E. Beyer, G. Herziger, and H. Kunze, Journal of Physics D **25**, 57-65 (1992).
- 40 B. R. Finke and G. Simon, Journal of Physics D **23**, 67-74 (1990).
- 41 J. F. Ziegler, Journal of Applied Physics **85**, 1249-72 (1999).
- 42 www.srim.org
- 43 R. K. Singh and J. Narayan, Physical Review B **41**, 8843-59 (1990).
- 44 R. K. Singh, O. W. Holland, and J. Narayan, Journal of Applied Physics **68**, 233-47 (1990).
- 45 R. Kelly, Journal of Chemical Physics **92**, 5047-56 (1990).
- 46 R. Kelly, Physical Review A **46**, 860-74 (1992).
- 47 A. Thum-Jaeger, B. K. Sinha, and K. P. Rohr, Physical Review E **6302**, 016405 (2001).
- 48 A. A. Voevodin and S. J. P. Laube, Surface & Coatings Technology **105**, 125-129 (1998).
- 49 R. Betti, V. N. Goncharov, R. L. McCrory, and C. P. Verdon, Physics of Plasmas **5**, 1446-
54 (1998).

- ⁵⁰ A. Ng, D. Pasini, P. Celliers, D. Parfeniuk, L. Da Silva, and J. Kwan, *Applied Physics Letters* **45**, 1046-8 (1984).
- ⁵¹ A. K. Sharma and R. K. Thareja, *Journal of Applied Physics* **88**, 7334-7338 (2000).
- ⁵² Y. B. Zel'dovich and Y. P. Raizer, *Physics of Shock Waves and High-Temperature Hydrodynamic phenomena* (Academic, New York, 1966).
- ⁵³ J. P. Zheng, Z. Q. Huang, D. T. Shaw, and H. S. Kwok, *Applied Physics Letters* **54**, 280-2 (1989).

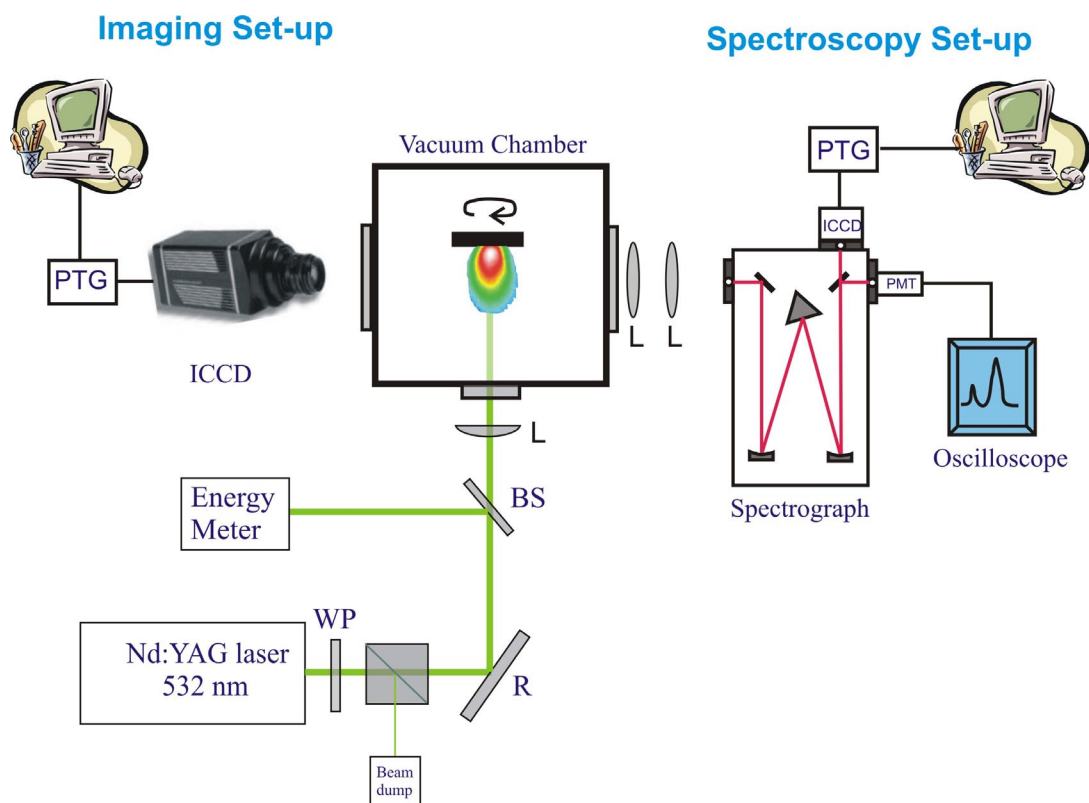


Fig.1. The schematic of the experimental set-up used for imaging and time resolved emission studies. (PTG, Programmable Timing Generator; PMT, Photomultiplier tube; WP, wave plate; R, reflector; BS, beam sampler; L, lens)

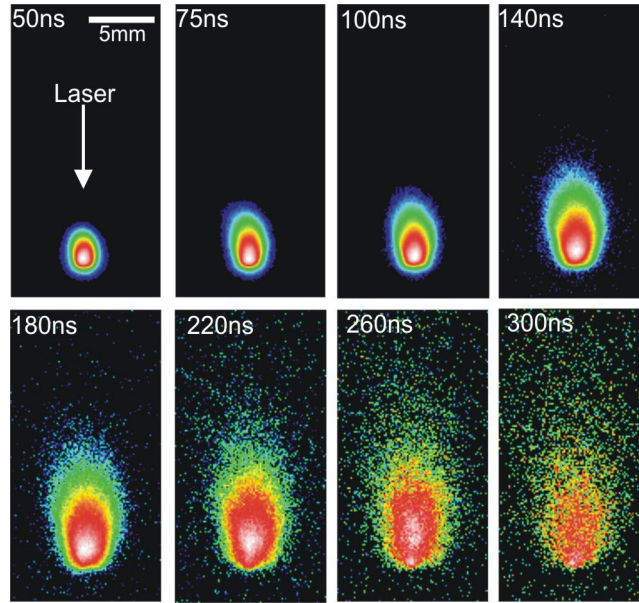


Fig. 2. The time evolution of visible emission from an aluminum plume recorded using an ICCD camera. The exposure time used was 2 ns. The laser power density used was 3 GWcm^{-2} and background pressure was 1×10^{-6} Torr. The timings in the images represent the time after the onset of plasma formation. All of the images are normalized to their maximum intensity. Plume behavior indicates free expansion.

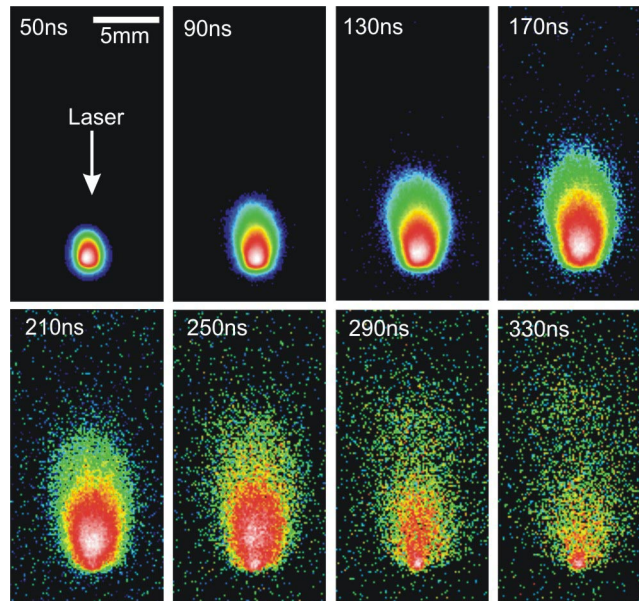


Fig.3. ICCD photographs of visible emission from laser produced aluminum plasma at 1×10^{-2} Torr background air pressure. The experimental parameters are the same as described in fig. 2. All of the images are normalized to their maximum intensity. Plume behavior shows free expansion.

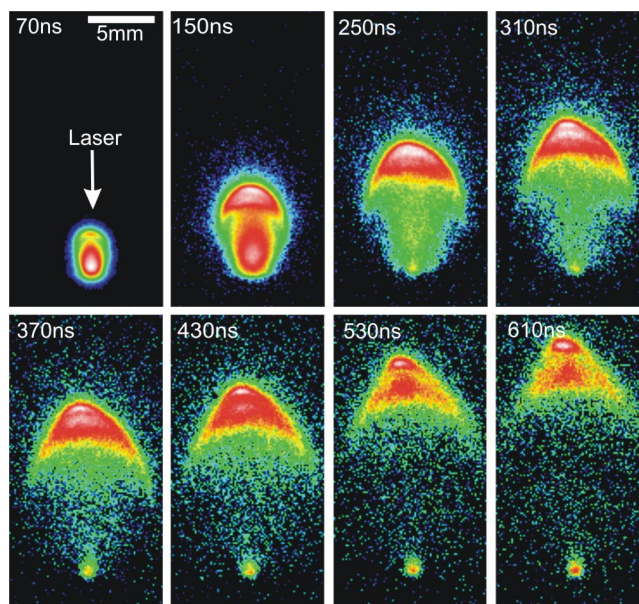


Fig.4. ICCD photographs of visible emission from laser produced aluminum plasma at 150mTorr background air pressure. The experimental parameters are the same as described in fig. 2. All of the images are normalized to their maximum intensity. Plume splitting and sharpening are observed in this pressure regime.

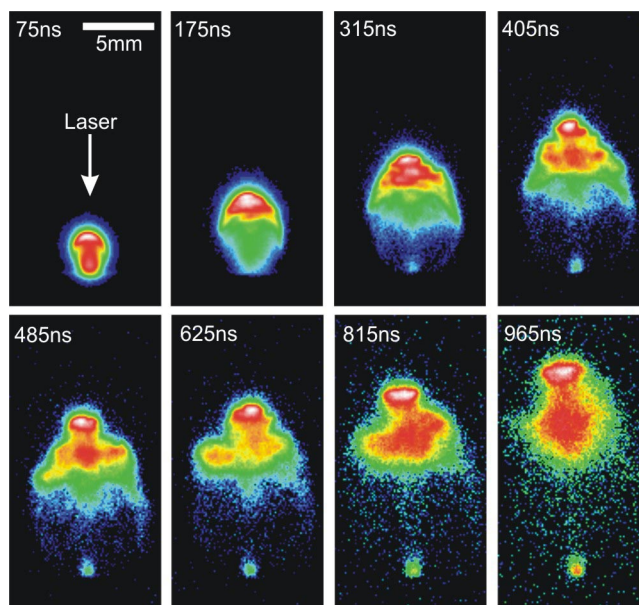


Fig.5. ICCD photographs of visible emission from Laser produced Aluminum plasma at 1.3 Torr background air pressure. The experimental parameters are the same as described in fig. 2. All the images are normalized to their maximum intensity. In this pressure regime, an instability is appeared as plasma expands into background gas.

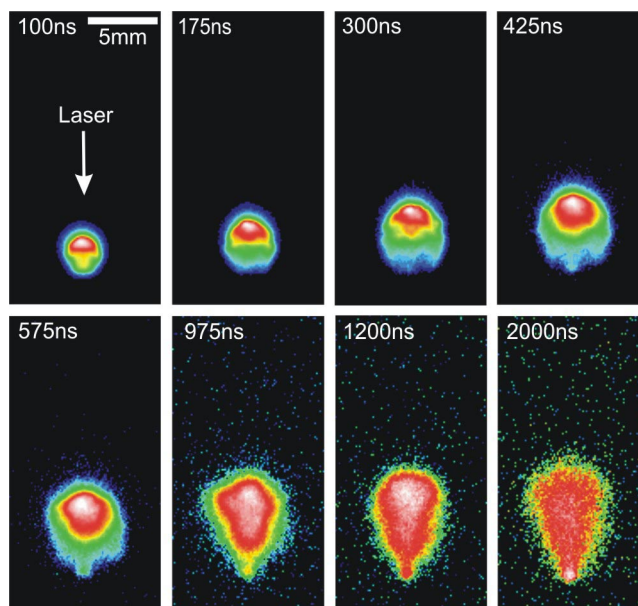


Fig.6. ICCD photographs of visible emission from laser produced aluminum plasma at 10 Torr background air pressure. The experimental parameters are the same as described in fig. 2. All of the images are normalized to their maximum intensity.

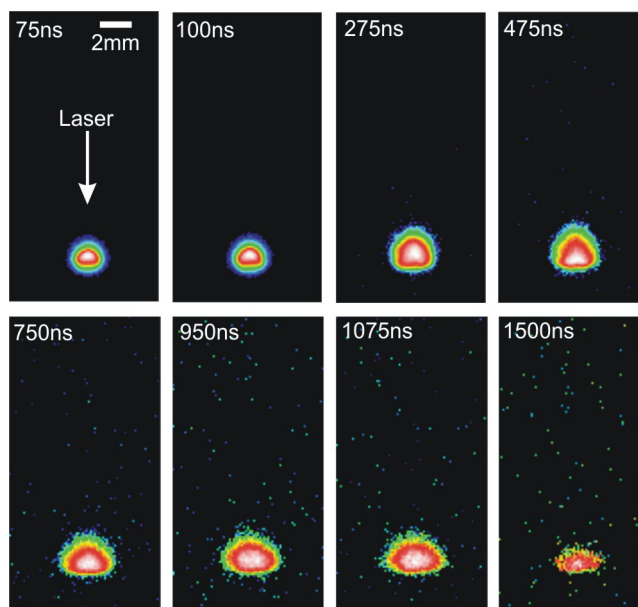


Fig.7. ICCD photographs of visible emission from laser produced aluminum plasma at 100 Torr background air pressure. The experimental parameters are the same as described in fig. 2. All of the images are normalized to their maximum intensity.

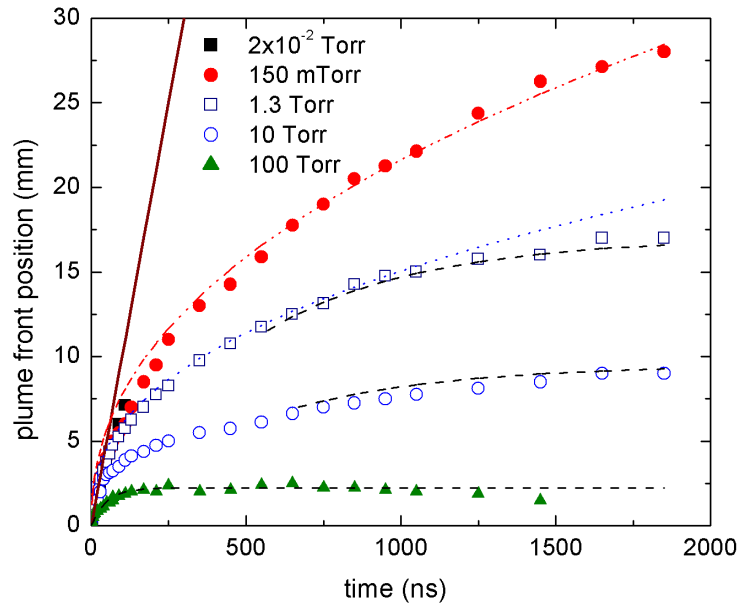


Fig. 8. Position-time (R-t) plots of the luminous front of the aluminum plume produced at different background air pressures measured from gated ICCD plume images. The symbols in the figure represent experimental data points and curves represent different expansion models. The solid line represents the free expansion ($R \propto t$). The dotted curve represents the shock wave model ($R \propto t^{0.4}$). The dashed curves show the drag model fit. The curve (dash dot) corresponding to 150 mTorr data is the best fit ($R \propto t^{0.445}$).

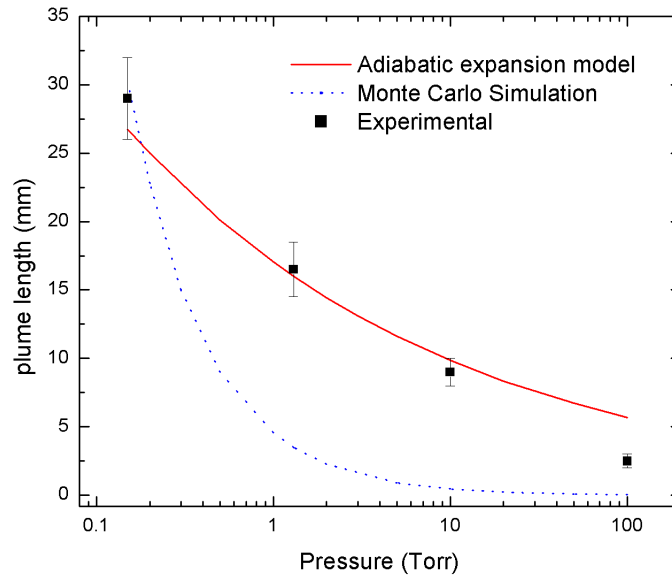


Fig. 9. Plume length vs pressure curves. The solid curve represents the plume length estimated for different pressures using adiabatic expansion model. The dotted curve shows the projected ion stopping distance at different pressure levels estimated using Monte Carlo Simulation. The symbols represent the experimental points.

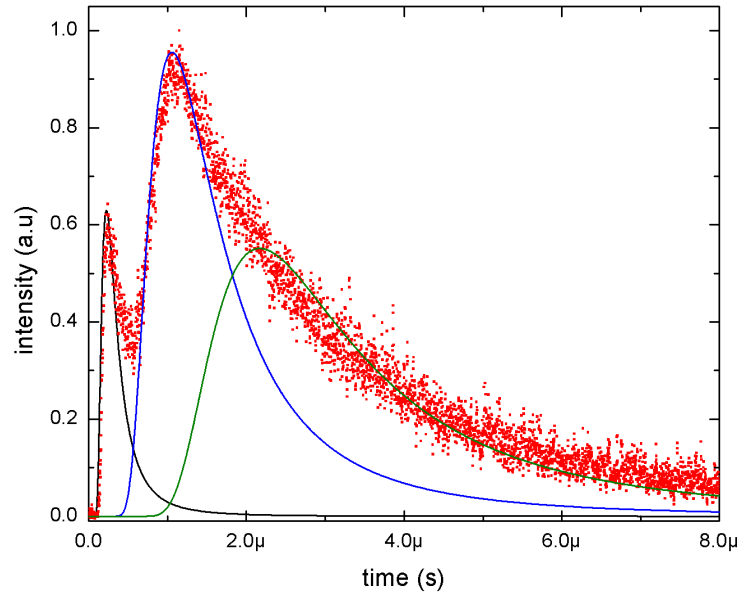


Fig.10. Intensity variation of spectral emission with time for Al species (396 nm) recorded at 18mm from the target surface. The laser power density used was 3 GWcm^{-2} and the background air pressure was 150 mTorr for these measurements. The solid lines represent the shifted Maxwell-Boltzmann fit as described in the text. The faster peak is fitted with simple Maxwell-Boltzmann distribution using $T = 650 \text{ eV}$. The fitting parameters for SMB distribution for the slow peaks are $T=28 \text{ eV}$ and $T = 7 \text{ eV}$ respectively.

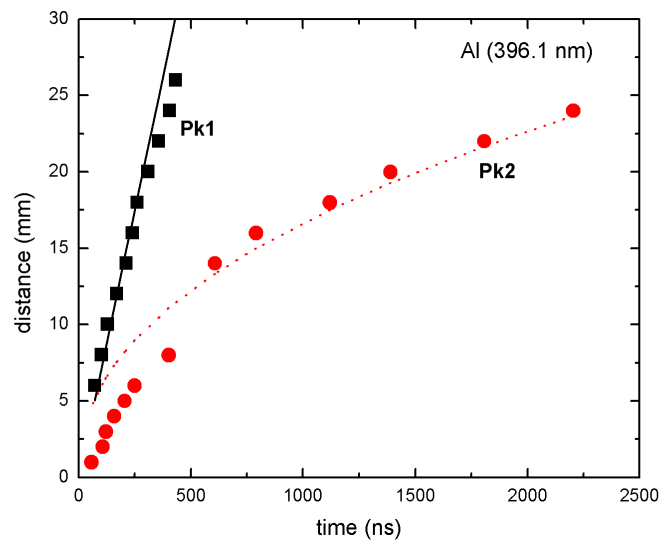


Fig. 11. Position-time graphs for two peaks observed with time resolved emission studies of Al species at 396.1 nm. Pk1 and Pk2 represent the faster and slower component respectively. The solid line corresponds to linear fit and the dotted curve is the fit for $R \propto t^{0.445}$.

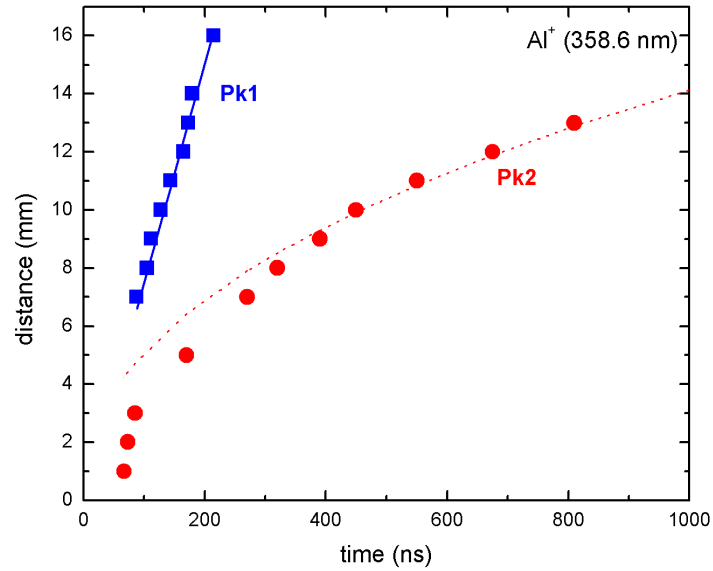


Fig.12. Position-time plots for faster (Pk1) and slower (Pk2) component in the temporal profiles of emission from Al⁺ species at 358.6 nm. The solid line in the figure corresponds to $R \propto t$ (free expansion) and the dotted curve represents the best fit ($R \propto t^{0.445}$).